


# Texture–Microstructure Correlation in Hot-Rolled AZ31

Hossein Aghamohammadi<sup>1</sup> · Seyed Jamal Hosseinipour<sup>1</sup> · Sayed Mahmood Rabiee<sup>1</sup> ·  
Roohollah Jamaati<sup>1</sup> 

Received: 4 December 2018 / Accepted: 26 February 2019 / Published online: 14 March 2019  
© The Indian Institute of Metals - IIM 2019

**Abstract** The paper presents a correlation between microstructure and crystallographic texture in hot-rolled AZ31 magnesium alloy. The microstructure and texture evolution are investigated using optical microscopy, field emission scanning electron microscopy, X-ray diffraction, respectively. The results indicated discontinuous dynamic recrystallization, twinning dynamic recrystallization, and particle stimulated nucleation as the main mechanisms during hot deformation. The average size of grains decreased from 19 to 1  $\mu\text{m}$  as the rolling reduction increased from 0 to 60%. A large area fraction of new grains was observed at 40% thickness reduction. At the beginning of plastic deformation, basal slip and extension twinning increased the intensity of  $\{0001\}$  basal fiber texture. Dynamic recrystallization had a considerable effect on weakening the basal texture. Interestingly, some unusual highly stable components including  $(01\bar{1}3)[7\bar{8}13]$ ,  $(01\bar{1}3)[\bar{2}110]$ , and  $(01\bar{1}3)[14\bar{5}3]$  existed at all deformation conditions and their intensity remained nearly unchanged.

**Keywords** Magnesium alloys · Hot rolling · Crystallographic texture

## 1 Introduction

Weight reduction can significantly decrease fuel consumption. For this reason, magnesium alloys have been increasingly used in the aerospace and automotive industries. These alloys possess high specific strength and good castability; however, their applications are hindered due to low formability [1–5]. This owes to the absence of independent slip systems at room temperature. The slip systems in magnesium alloys are  $\{0001\}\langle 11\bar{2}0\rangle$  basal,  $\{10\bar{1}0\}\langle 11\bar{2}0\rangle$  prismatic,  $\{10\bar{1}1\}\langle 11\bar{2}3\rangle$  first-order pyramidal, and  $\{11\bar{2}2\}\langle 11\bar{2}3\rangle$  second-order pyramidal. In addition to slip, mechanical twinning has a significant contribution to plastic deformation of magnesium alloys. The main twinning systems in magnesium alloys are  $\{10\bar{1}2\}\langle \bar{1}011\rangle$  extension and  $\{10\bar{1}1\}\langle 10\bar{1}2\rangle$ ,  $\{10\bar{1}3\}\langle 10\bar{1}2\rangle$  or  $\{10\bar{1}5\}\langle 10\bar{1}2\rangle$  contraction. Sometimes, a new twin nucleates inside a primary twin. This mechanism is double (or secondary) twinning. The main double twinning systems in magnesium alloys are  $\{10\bar{1}1\} - \{10\bar{1}2\}$  or  $\{10\bar{1}3\} - \{10\bar{1}2\}$ , i.e., the contraction twin is followed by the extension one [1–6].

The crystallographic texture is an important effect on the performance of magnesium alloys. Data on the correlation of microstructure with the preferred orientation of magnesium alloys can be found in the literature [1–5, 7, 8]. Guan et al. [7] investigated the effect of recrystallization nucleation sites on texture weakening in the AZ31 alloy. The  $\{10\bar{1}1\} - \{10\bar{1}2\}$  double twins were the preferential nucleation sites for recrystallization and made the main contribution to recrystallized texture. Su et al. [3] also stated that the basal pole splitting along the rolling direction is generated in a hot-rolled AZ31 alloy that is related to contraction and double twinning. Gou et al. [8] indicated that the dynamically recrystallized grains in the hot-rolled

✉ Roohollah Jamaati  
jamaati@nit.ac.ir

<sup>1</sup> Department of Materials Engineering, Babol Noshirvani University of Technology, Shariati Ave., Babol 47148–71167, Iran

AZ91 alloy are smaller and weaken the preferred orientation. Increasing deformation up to 60% leads to a significant enhancement of dynamic recrystallization in the AZ91 alloy, which results in a texture weakness.

It is essential to completely understand the correlation of microstructure with the crystallographic texture of magnesium alloys during plastic deformation. In the present study, the microstructure and texture evolution of AZ31 alloy subjected to hot rolling are investigated and the corresponding mechanisms are studied and discussed.

## 2 Experimental Procedure

The material used in the present work is the commercially available magnesium alloy AZ31 plate with 12.4 mm thickness. The plate firstly homogenized at 450 °C for 6 h. The homogenized samples, then, preheated at 450 °C for about 15 min before rolling. The hot plate was rolled with reduction of 10% for each pass. The number of passes were 1, 4, and 6 corresponding to the total thickness reductions of 10, 40, and 60%, respectively. Each time, the plate was reheated to the specified temperature before the next pass.

Microstructural and texture analysis was performed on the RD–TD plane of samples. The microstructures were observed using optical microscope (OM) and field emission scanning electron microscope (FESEM). For metallography, the samples were mechanically ground with a series of SiC papers followed by polishing. The acetic-picral solution was used as an etchant to show the grain structure. For macrotexture characterization, X-ray diffraction (XRD) measurements were conducted and the results were analyzed by TexTools software (ResMat Co.). The size of the

samples for texture measurement was 15 mm in length and 10 mm in width. The  $\{0002\}$  and  $\{10\bar{1}0\}$  incomplete pole figures were measured.

## 3 Results and Discussion

The FESEM micrograph of as-homogenized AZ31 sample is presented in Fig. 1a. Figure 1b shows EDS spectra of the particle as indicated by arrow in Fig. 1a. The EDS confirms that the intermetallic particle is  $\beta$ -Mg<sub>17</sub>Al<sub>12</sub> phase. Figure 2 shows the optical micrographs of the as-homogenized and hot-rolled samples in the RD–TD plane. As shown in Fig. 2a, the microstructure of the as-homogenized sample consists of Mg<sub>17</sub>Al<sub>12</sub> particles and coarse equiaxed  $\alpha$ -Mg grains with an average size of 19  $\mu$ m and a large number of twins. In this sample, there are two types of twins including  $\{10\bar{1}2\}$  extension twin (ET) with thick and lenticular morphology and  $\{10\bar{1}1\}$  contraction twin (CT) with thin and extended morphology. Figure 2b–d demonstrates the microstructures of AZ31 after 10, 40, and 60% hot rolling, respectively. As shown in Fig. 2b, when the AZ31 is subjected to a thickness reduction of 10%, the number of ET and CT is increased. However, the amount of the extension twins is much higher than that of the contraction twins. This is due to smaller critical resolved shear stress (CRSS) of the ETs when compared to the CTs. It is reported that the  $\{10\bar{1}2\}$  twinning requires only 2–3 MPa while the  $\{10\bar{1}1\}$  one requires 76–153 MPa [9]. For this reason, extension twinning together with basal slip can be activated in the early stage of deformation (uniform deformation). Figure 1b clearly shows that a maximum volume fraction of extension twins is achieved. In addition,

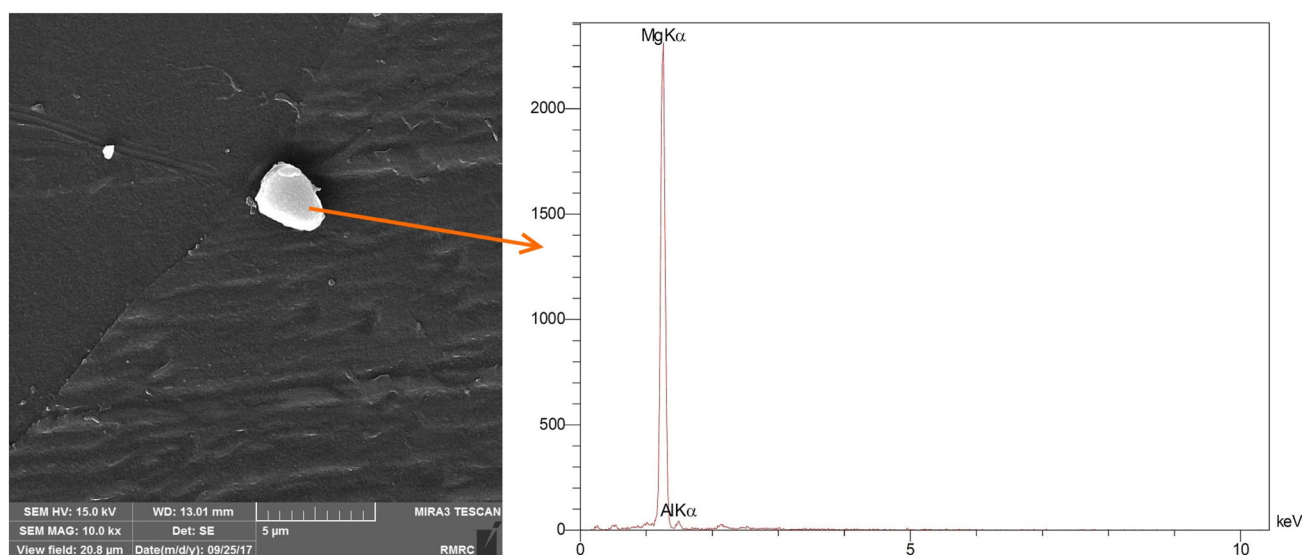


**Fig. 1** EDS spectrum from second phase particle in the as-homogenized AZ31 alloy

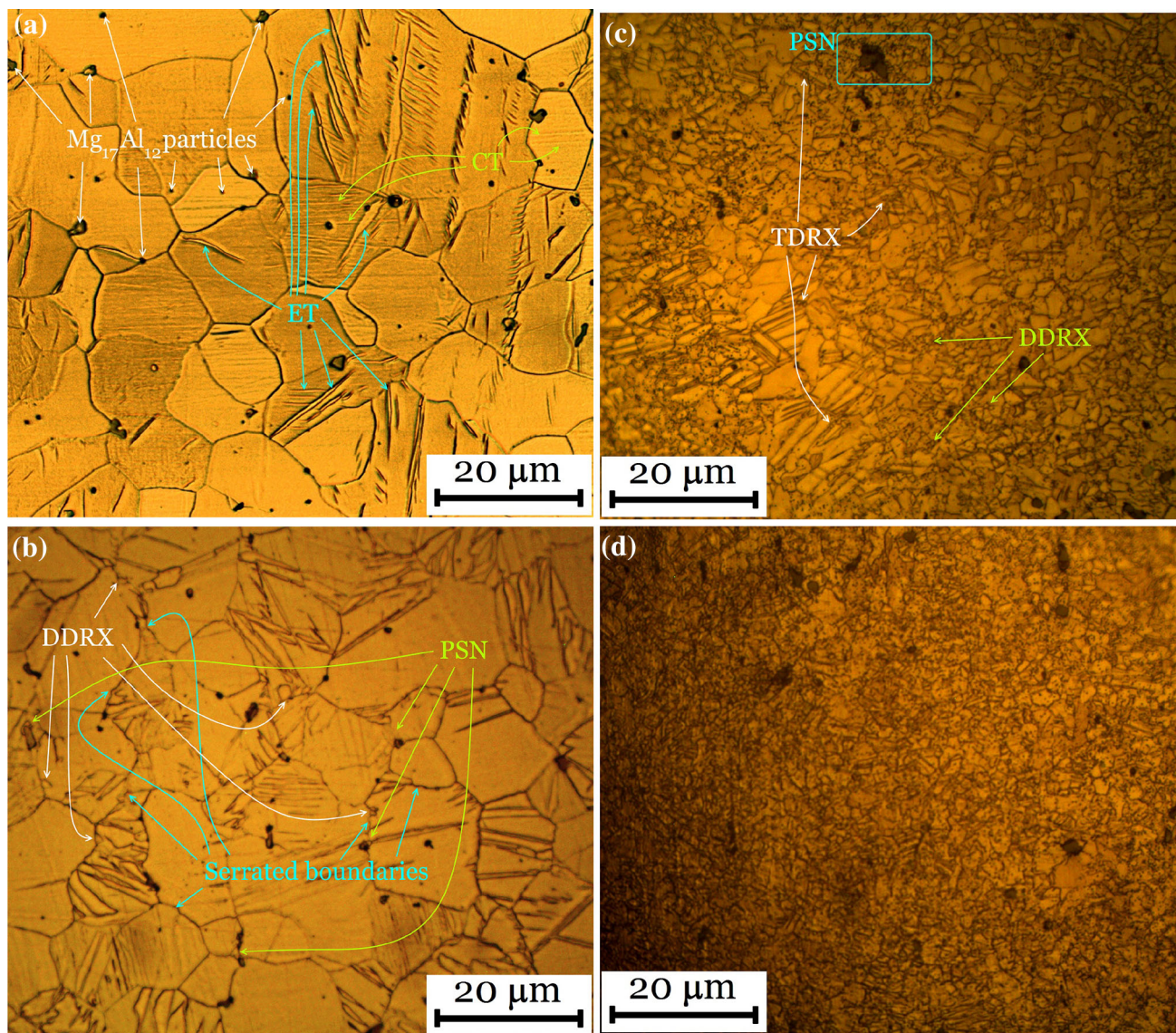


**Fig. 2** Microstructures of **a** as-homogenized, **b** 10%, **c** 40%, and **d** 60% hot-rolled samples

a few cross-twins are created. One can also observe that the twin size increases as a result of multiple nucleation events followed by growth and coalescence of twin boundaries. However, the growth rate of ETs is higher than that of CTs. At the rolling reduction of 40% and 60%, as shown in Fig. 2c, d, the amount of extension twins significantly decreases as deformation increases and the contraction and cross-twins are observed. When rolling reduction is increased, the plastic deformation is induced by the contraction and cross-twinning that is not homogeneous.

From Fig. 2, the average grain sizes after hot rolling at 10% and 60% thickness reductions are about 15 μm and 1 μm, respectively. It should be noted that there is a bimodal distribution in Fig. 1c, in which case an average grain size may not have much validity. The grain refinement is observed in all deformation conditions due to

dynamic recrystallization (DRX). There are four mechanisms proposed in the literature that account for dynamic recrystallization in magnesium alloys including continuous dynamic recrystallization (CDRX), discontinuous dynamic recrystallization (DDRX), twinning dynamic recrystallization (TDRX), and particle stimulated nucleation (PSN) [1–8]. In order to recognize the DRX type in the hot-rolled AZ31, investigation of misorientation angle between grains is essential. The distribution of misorientation angle as a function of thickness reductions is plotted in Fig. 2. It is defined that high angle grain boundaries (HAGBs) have misorientations larger than 15°, and the low angle grain boundaries (LAGBs) have misorientations lower than 15°. As shown in Fig. 3, the volume fraction of grains with LAGBs after 0, 10, 40, and 60% hot rolling are 2.1, 2.7, 3.7, and 5.3%, respectively. It is found that the volume

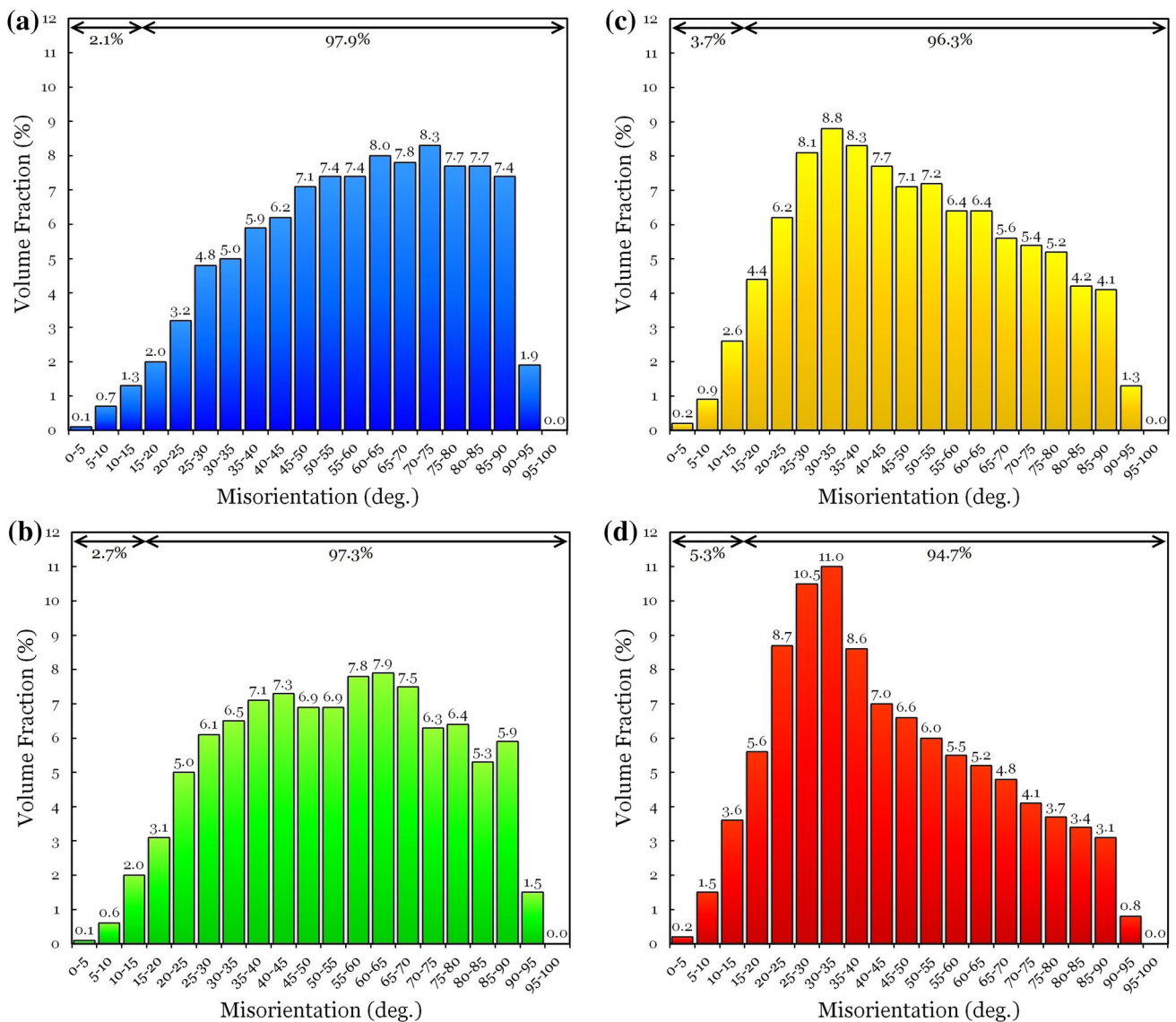


**Fig. 3** Misorientation distributions of **a** as-homogenized, **b** 10%, **c** 40%, and **d** 60% hot-rolled samples

fraction of grains with low angle grain boundaries increases with rolling reduction.

Figure 2b indicates the migration of grain boundaries and generation of serrated/wavy grain boundaries and some new grains formed near to the serrated boundaries. In general, the grain boundaries act as obstacles to the dislocation motion. Therefore, the grain boundaries accumulate dislocations leading to increasing the local stress and formation of serrated boundaries. The development of serrated/wavy boundaries results in the nucleation of new grains through bulging. This type of recrystallization mechanism is considered as discontinuous dynamic recrystallization mechanism.

In addition to DDRX to produce new grains, Fig. 2b demonstrates that the dynamic recrystallization behavior of AZ31 after 10% hot rolling is also associated with particle

stimulated nucleation phenomenon. The  $Mg_{17}Al_{12}$  intermetallic particles are responsible for dynamic recrystallization through PSN mechanism. Three conditions must be satisfied for the particle stimulated nucleation mechanism to take place. First, a heterogeneous deformation zone must be created around the  $Mg_{17}Al_{12}$  intermetallic particle. Second, the magnesium must have high enough stored energy density for a recrystallized nucleus to grow away from the  $Mg_{17}Al_{12}$  particle. Third, the  $Mg_{17}Al_{12}$  particle diameter should be greater than  $1\ \mu m$  [10]. During hot rolling of AZ31, a mismatch in the deformation of deformable magnesium and large undeformable (unsharable)  $Mg_{17}Al_{12}$  particles enhances the dislocation density near the matrix/particle interface. This can generate a high driving force in the vicinity of the large particles for nucleation of new grains.

The grain refinement in the 40% and 60% hot-rolled AZ31, as shown in Fig. 2c, d, is more intense than in the 10% deformed sample due to the more severe process of DDRX and PSN. In addition to discontinuous dynamic recrystallization and particle stimulated nucleation to create new grains, Fig. 2c, d indicates that the DRX of magnesium after 40% and 60% deformations is also associated with the twinning dynamic recrystallization mechanism. Increasing dislocation density during plastic deformation of AZ31 results in storing a large amount of energy inside contraction twins. To reduce the stored energy, the double twins are formed inside the primary contraction twins and some subgrains are formed inside the twinned regions [6, 7]. In fact, the subgrains divide both contraction and double twins into small parts, in which new grains nucleate due to high dislocation density. This is the twinning dynamic recrystallization mechanism.

Figures 4 and 5 show recalculated  $\{0002\}$  pole figures (PFs) and orientation distribution functions (ODFs) of the hot-rolled AZ31 after 0, 10, 40, and 60% thickness reductions, respectively. It should be noted that no basal pole splitting along the rolling or transverse direction is

observed under all deformation conditions. Figures 4a and 5a indicate that the  $\{0001\}$  basal texture is dominant in which the  $\langle 0001 \rangle$  of grains is nearly parallel to the normal direction. Meanwhile, the peak intensity of as-homogenized sample for PF and ODF are  $8.4 \times R$  and  $9.4 \times R$ , respectively. It should be noted that some grains don't have the basal fiber texture. They have strong  $\{11\bar{2}3\}$ , moderate  $\{10\bar{1}1\}$ , and weak  $\{10\bar{1}3\}$  fiber textures as shown in Fig. 5. The subsequent rolling deformation reorients the  $c$ -axis of more grains towards normal direction leading to increase in the  $\{0001\}$  basal texture intensity (see Fig. 4b). As seen, the maximum intensity of AZ31 after 10% hot rolling for PF and ODF is enhanced to  $9.4 \times R$  and  $10.0 \times R$ , respectively. Increasing the intensity of  $\{0001\}$  basal texture is mainly due to  $\{0001\}$  basal slip and  $\{10\bar{1}2\}$  extension twin at the early stages of plastic deformation. Activation of basal slip and extension twin at the beginning of the deformation is very easy due to their lower CRSS than  $\{10\bar{1}0\}$  prismatic slip,  $\{10\bar{1}1\}$  or  $\{11\bar{2}2\}$  pyramidal slips,  $\{10\bar{1}1\}$  or  $\{10\bar{1}3\}$  contraction twin, and  $\{10\bar{1}1\} - \{10\bar{1}2\}$  double twin [6, 9]. As shown in Fig. 2b, with increasing the rolling reduction to 10%, more extension

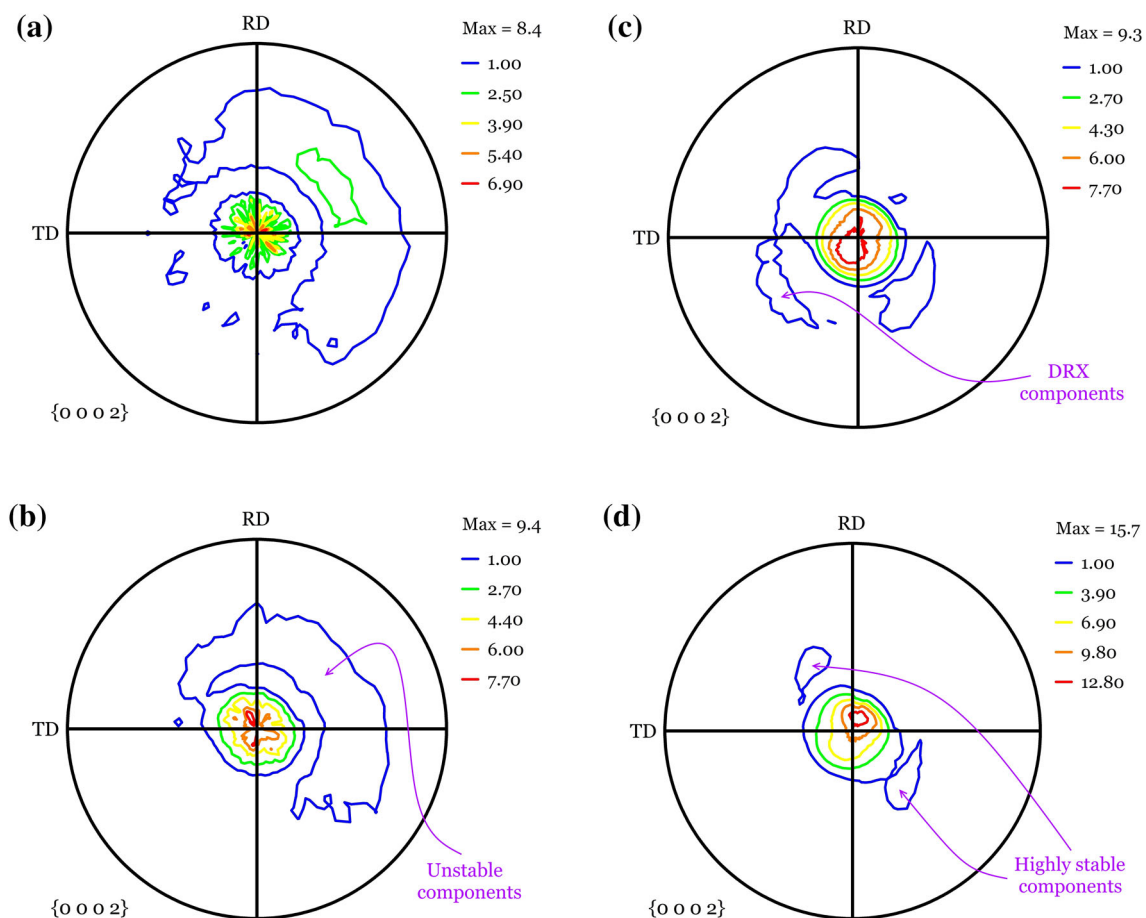


**Fig. 4** Pole figures of **a** as-homogenized, **b** 10%, **c** 40%, and **d** 60% hot-rolled samples

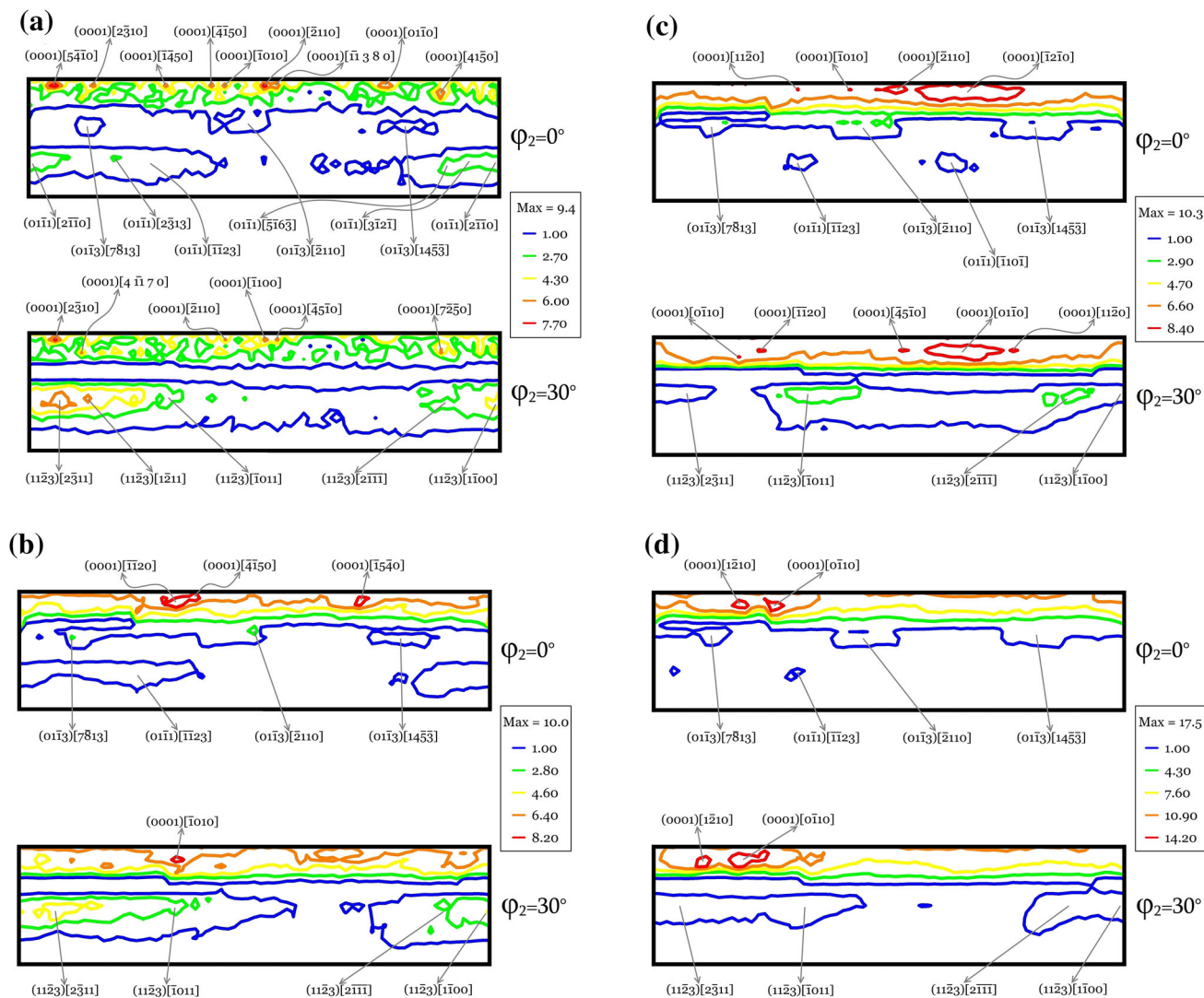


**Fig. 5** ODFs of **a** as-homogenized, **b** 10%, **c** 40%, and **d** 60% hot-rolled samples

twins are formed and developed which accommodate plastic strain along  $\langle 0001 \rangle$ . Extensive formation and development of  $\{10\bar{1}2\}$  extension twins result in a reorientation of grains by  $86.3^\circ$  about  $\langle 11\bar{2}0 \rangle$  which rotates the basal poles parallel to the normal direction [3, 6]. In other words, rolling deformation reorients the  $\langle 0001 \rangle$  direction of grains parallel to the ND. As shown in Fig. 5b, the intensity of  $\{11\bar{2}3\}$  and  $\{10\bar{1}1\}$  fibers is reduced, but  $\{10\bar{1}3\}$  is stable. In fact,  $\{11\bar{2}3\}$  and  $\{10\bar{1}1\}$  fibers are unstable textures that may be eliminated by increasing the reduction in thickness (see Fig. 4b). Figures 4c and 5c indicate that the intensity of  $\{11\bar{2}3\}$  fiber get weakened again and that of  $\{10\bar{1}1\}$  fiber almost disappears, while the weak  $\{10\bar{1}3\}$  texture, i.e.,  $(01\bar{1}3)[7\bar{8}13]$ ,  $(01\bar{1}3)[2\bar{1}10]$  and  $(01\bar{1}3)[14\bar{5}\bar{3}]$  components are stable yet. On the other hand, interestingly the intensity of  $\{0001\}$  fiber remains nearly unchanged (i.e.,  $9.3 \times R$  and  $10.3 \times R$  for PF and ODF, respectively). This appears to be due to the occurrence of intense

dynamic recrystallization at 40% hot rolling of AZ31 alloy (see Fig. 2c). The new grains created by CDRX, DDRX, TDRX, and PSN mechanisms without preferred orientation can effectively weaken the basal texture. At this time, however, the other mechanisms (i.e., basal slip and extension twinning) have no considerable effect on texture evolution. It can be concluded that the DRX plays important role in weakening the crystallographic texture [3, 7, 8]. After the rolling reduction of 60% (Figs. 4d, 5d), a very strong basal fiber texture is generated. It is clearly seen that the maximum intensity of samples after 60% hot rolling for PF and ODF enhance to  $15.7 \times R$  and  $17.5 \times R$ , respectively. The hot rolling deformation reorients the previous new recrystallized grains (Fig. 2c) toward  $\{0001\}$  basal texture due to basal slip at the final steps of hot deformation. Besides the severe basal texture, however, there are weak  $(01\bar{1}3)[7\bar{8}13]$ ,  $(01\bar{1}3)[2\bar{1}10]$ , and

$(01\bar{1}3)[14\bar{5}\bar{3}]$  texture components again. This finding is very surprising. These uncommon highly stable texture components exist for all samples, and its intensity remains almost unchanged. It can be concluded that if some grains in AZ31 alloy rotate toward  $(01\bar{1}3)[7\bar{8}13]$ ,  $(01\bar{1}3)[\bar{2}110]$ , and  $(01\bar{1}3)[14\bar{5}\bar{3}]$  components (i.e.,  $\{10\bar{1}3\}$  fiber), more rotation is impossible.

#### 4 Conclusions

Correlation between texture and microstructure of AZ31 alloy during hot rolling was investigated. The following conclusions could be made:

1. Average grain size decreased from 19 to 1  $\mu\text{m}$  with increasing thickness reduction from 0 to 60%.
2. Texture weakening was observed after 40% deformation as a result of intense DRX.
3. Increasing the deformation led to an increase in the texture intensity of the basal planes (0001) parallel to ND by basal slip and extension twinning.
4. Surprisingly, there were some unexpected highly stable components including  $(01\bar{1}3)[7\bar{8}13]$ ,  $(01\bar{1}3)[\bar{2}110]$ , and  $(01\bar{1}3)[14\bar{5}\bar{3}]$  at all rolling reductions, and their intensity remained nearly unchanged.

**Acknowledgements** The authors acknowledge the funding support of Babol Noshirvani University of Technology through Grant Program Nos. BNUT/370203/98, BNUT/370388/98, and BNUT/393044/98.

#### References

1. Xu W, Birbilis N, Sha G, Wang Y, Daniels J E, Xiao Y, and Ferry M, *Nat Mater* **14** (2015) 1229.
2. Kim D G, Lee K M, Lee J S, Yoon Y O, and Son H T, *Mater. Lett.* **75** (2012) 122.
3. Su J, Sanjari M, Kabir A S H, Jung I H, Jonas J J, Yua S, and Utsunomiya H, *Mater Sci Eng A* **636** (2015) 582.
4. Li Q, and Tian B, *Mater Lett* **67** (2012) 81.
5. Zhang Z, *Mater Lett* **116** (2014) 131.
6. Ostapovets A, Bursik J, Krahula K, Kral L, and Serra A, *Philos Mag* **97** (2017) 1088.
7. Guan D, Rainforth W M, Gao J, Sharp J, Wynne B, and Ma L, *Acta Mater* **135** (2017) 14.
8. Guo F, Zhang D, Wu H, Jiang L, and Pan F, *J Alloys Compd* **695** (2017) 396.
9. Koike J, *Metall Mater Trans A* **36** (2005) 1689.
10. Humphreys J, Rohrer G S, and Rollett A, *Recrystallization and Related Annealing Phenomena*, Third Edition, Elsevier, Oxford (2017).

**Publisher's Note** Springer Nature remains neutral with regard to jurisdictional claims in published maps and institutional affiliations.